9-(p-Tolyl)-2,3,4,4a,9,9a-hexahydro-1H-carbazole – a new donor building-block in the design of sensitizers for dye-sensitized solar cells

9-(*p*-Tolyl)-2,3,4,4a,9,9a-hexahydro-1*H*-carbazole – a new donor building-block in the design of sensitizers for dye-sensitized solar cells

Maxim S. Mikhailov[a], Nikita S. Gudim[b], Ekaterina A. Knyazeva[a,b], Ellie Tanaka,[c] Lu Zhang [c], Ludmila V. Mikhalchenko[b], Neil Robertson[c,*], Oleg A. Rakitin[a,b,*]

[a]*Nanotechnology Education and Research Center, South Ural State University, 454080 Chelyabinsk, Russia*

[b]*N. D. Zelinsky Institute of Organic Chemistry, Russian Academy of Sciences, 119991 Moscow, Russia*

[c]*EaStCHEM School of Chemistry, University of Edinburgh, Edinburgh EH9 3FJ, UK*

Abstract

The novel donor building-block - 9-(*p*-tolyl)-2,3,4,4a,9,9a-hexahydro-1*H*-carbazole was designed and employed in the synthesis of dye-sensitized solar cell (DSSCs). An effective, high-yielding synthesis of 4,6-(4,4,5,5-tetramethyl-1,3,2-dioxaborolan-2-yl)-9-(p-tolyl)-1,2,3,4,4a,9a-hexahydrocarbazole from 1,2,3,4,4a,9a-hexahydrocarbazole was realized. Three new metal-free organic sensitizers, containing the new donor building block were prepared by a stepwise approach from 4,7-dibromobenzo[c][1,2,5]chacogenadiazoles. A 2,1,3-Benzothiadiazole dye containing hexahydrocarbazole donor, thiophene as π-spacer and cyanoacrylate as anchoring electron acceptor showed photovoltaic properties higher than the well-known **WS-2** sensitizer with PCE = 5.86%. Although benzoxa- and –selenadiazole dyes have a bathochromic shift (24-30 nm) in the UV-vis spectra, and smaller energy gap E_g (about 0.1 eV), they have lower photovoltaic parameters, including PCE of 1.5-2.3%. Introducing a new donor 9-(*p*-tolyl)-2,3,4,4a,9,9a-hexahydro-1*H*-carbazole into the construction of the DSSCs has broadened possibilities for the optimization of their photovoltaic properties.

Corresponding author. Tel.: +7-499-135-53-27; fax: +7-499-135-53-28; e-mail: orakitin@ioc.ac.ru; neil.robertson@ed.ac.uk.

Keywords: dye-sensitized solar cells; 9-(*p*-tolyl)-2,3,4,4a,9,9a-hexahydro-1*H*-carbazole; power conversion efficiency; 2,1,3-benzochalcogenadiazoles

1. Introduction

In the last couple of decades, dye-sensitized solar cells (DSSCs) have attracted worldwide research attention due to their potential for low cost production, easy fabrication and relatively high power conversion efficiency [1-3]. A dye sensitizer, a photoanode, a redox electrolyte and a counter electrode are the essential components for a typical DSSC. Among other components of DSSCs, the dye sensitizer is responsible for harvesting sunlight, initiating charge transfer, and injecting electrons into the photoanode. Efficient sensitizers have been developed based on ruthenium polypyridine complexes, zinc porphyrins [4-6] and metal-free organic dyes, among which the latter have been most intensively investigated [7-11]. Most typical organic dyes are designed with a donor-π-bridge-acceptor (D-π-A) configuration due to easy synthesis and efficient intramolecular charge transfer (ICT) properties [12-15]. The electronic interaction between donor (D) and acceptor (A) results in strong charge-transfer absorption bands that harvest sunlight for photon-to-electron conversion. Recently, Zhu and Tian proposed a new concept of the D–A–π–A motif for designing a generation of stable and efficient organic dyes [16-18]. Compared to D–π–A dyes, the properties of D–A–π–A dyes can be readily adjusted by incorporation of an auxiliary acceptor between the donor and π-bridge, which broadens the absorption and enhances efficient ICT for high performance DSSCs [19]. Some electron-withdrawing heterocyclic systems, such as diketopyrrolopyrrole, benzotriazole, benzothiadiazole, quinoxaline, benzoselenadiazole, pyridazinothiadiazole and many others have been used to design a D-A-π-A framework [20-25]. It was reported that the auxiliary acceptor is beneficial for extending absorption wavelength and enhancing the electron coupling, thus greatly improving photovoltaic properties and the stability of organic sensitizers [18]. Furthermore, the evolution of the π-bridge unit is essential in the molecular engineering of sensitizers, due to enhanced light absorption and photoinduced charge separation, as well as delayed charge recombination [26]. The most common electron withdrawing group widely employed as terminal acceptor is cyanoacrylic acid due to its strong binding on the surface of mesoporous TiO_2 through carboxylic acid anchoring groups [27]. Various other molecular engineering methods to improve the light harvesting efficiency of organic dyes involve an increase in the electronic richness of the donor moieties [28]. Introduction of electron-rich moieties on the donor segment helps to broaden the absorption spectra, and attachment of energy delocalizing chromophores causes prolongation of excited state lifetime and facilitates the electron injection into the conduction band of TiO_2 [29]. In general, triarylamine, indoline, tetrahydroquinoline, phenothiazine, phenoxazine are routinely used as donors [30]. 4-(*p*-

Tolyl)-1,2,3,3a,4,8b-hexahydrocyclopenta[*b*]indole donor has been shown to be one of the most effective donors [20,22]. A few attempts to modify this moiety with a change of *p*-tolyl to other aryl groups have been made [31-39], but they have not achieved significant success.

In this work we aimed to design a new donor building block - 9-(*p*-tolyl)-2,3,4,4a,9,9a-hexahydro-1*H*-carbazole, which is varied from 4-(*p*-tolyl)-1,2,3,3a,4,8b-hexahydrocyclopenta[*b*]indole by one extra CH_2 group, and to investigate the influence of this group on the photovoltaic properties of the organic sensitizers. Three novel dyes with various chalcogen atoms (oxygen, sulfur and selenium) in 2,1,3-benzochalcogenadiazole internal acceptor were synthesized and studied. The optical, electrochemical and photophysical properties of these dyes were investigated to disclose important design criteria for the discovery of further new organic dyes.

2. Experimental details

2.1. Materials

The reagents were purchased from commercial sources and used as received. Solvents were purified by distillation from the appropriate drying agents.

2.2.Synthesis and characterization of compounds:

*2.2.1. Synthesis of 4,6-(4,4,5,5-tetramethyl-1,3,2-dioxaborolan-2-yl)-9-(p-tolyl)-1,2,3,4,4a,9a-hexahydrocarbazole **4**.*

*2,9-(p-Tolyl)-1,2,3,4,4a,9a-hexahydrocarbazole **2**.*

In 50 ml round-bottom flask, 1,2,3,4,4a,9a-hexahydrocarbazole **1** (520 mg, 3 mmol), *p*-bromotoluene (513 mg, 3 mmol), cesium carbonate (1.36 g, 4.2 mmol), palladium acetate (3.5 mg, 15μmol), tris-*tert*-butylphosphine (72 μl, 0.3 mmol) and 10 ml dry xylene were added. After boiling for 20 h under argon, the mixture was diluted with petroleum ether and purified on a silica gel column to obtain colorless oil, **2** (715 mg, 80%). ^{1}H NMR (300 MHz, δ, ppm): 7.24 (m, 4H), 7.20 (d, J=2.8 Hz, 1H), 7.10 (t, J=7.6 Hz, 1H), 6.82 (t, J=7.6 Hz, 1H), 6.80 (d, J=7.6 Hz, 1H), 4.10 (m, 1H), 3.28 (m, 1H), 2.43 (s, 3H), 1.91-1.72 (m, 4H), 1.63-1.57 (m, 2H), 1.50-1.42 (m, 2H). ^{13}C NMR (75 MHz, δ, ppm): 149.36, 141.05, 134.91, 133.04, 129.87, 126.98, 123.18, 123.02, 118.62, 109.02, 64.66, 40.64, 28.25, 25.89, 22.92, 21.30, 20.95. HRMS-ESI (m/z): $[M]^+$ calcd for ($C_{19}H_{21}N$) 263.1667, found 263.1670, $[M+H]^+$ calcd for ($C_{19}H_{22}N$) 264.1747, found 264.1744. IR, ν, cm^{-1}: 3404, 2939, 2905, 2846, 1579, 1470, 1435, 1311, 1273, 1233, 1047, 971, 862, 798, 586, 485. R_f=0.41 (petroleum ether/ ethylacetate = 25:1).

*3,6-Bromo-9-(p-tolyl)-1,2,3,4,4a,9a-hexahydrocarbazole **3**.*

To a solution of **2** (450 mg, 1.7 mmol) and DMSO (133µl, 1,9 mmol) in 15 ml ethylacetate was added dropwise hydrobromic acid (48%, 0.45 ml, 3.76 mmol) at 60 ºC. After 5 minutes K_2CO_3 was added (300 mg) and the mixture was stirred another 1 h. After cooling down to room temperature the mixture was diluted with ethyl acetate, washed with water, and evaporated under reduced pressure. The organic layer was evaporated, the residue was purified on a silica gel column with petroleum ether to obtain colorless oil, **3** (494 mg, 85%). The sample was used in the next step as it is.

*4,6-(4,4,5,5-Tetramethyl-1,3,2-dioxaborolan-2-yl)-9-(p-tolyl)-1,2,3,4,4a,9a-hexahydrocarbazole **4**.*

In 25 ml round-bottom flask compound **3** (480 mg, 1.4 mmol), B_2Pin_2 (540 mg, 2.14 mmol), and potassium acetate (480 mg) were dissolved in 10 ml of dioxane. The solution was degassed for 20 minutes with a stream of argon, Pd_2dba_3 (9.5 mg, 10 µmol) and X-Phos (20 mg, 40 µmol) were added simultaneously. The reaction was then brought to 80 °C for 8 h, and then diluted with ethylacetate and filtered through a thin pad of celite. The mixture was evaporated and the compound purified on a silica gel column with a ethylacetate/petroleum ether mixture 1/50 as eluent to obtain a pale yellow oil, **4** (450 mg, 82%). ^{1}H NMR (300 MHz, δ, ppm): 7.66 (s, 1H), 7.63 (d, J=8 Hz, 1H), 7.23 (q, J=8.5 Hz, 4H), 6.77 (d, J=7.9 Hz, 1H), 4.12 (m, 1H), 3.28 (m, 1H), 2.42 (s, 3H), 1.91-1.72 (m, 4H), 1.63-1.57 (m, 2H), 1.41 (m, 14H). ^{13}C NMR (75 MHz, δ, ppm): 152.15, 140.28, 135.04, 134.01, 133.54, 129.93, 129.49, 123.37, 108.14, 83.23, 64.77, 40.31, 27.97, 25.89, 25.00, 24.83, 22.75, 21.22, 20.98. HRMS-ESI (m/z): $[M+H]^+$ calcd for ($C_{25}H_{32}NBO_2$) 390.2603, found 390.2603. IR, ν, cm^{-1}: 3237, 2929, 2858, 1603, 1515, 1460, 1382, 1233, 1198, 815, 739, 642. R_f = 0,34 (petroleum ether/ ethylacetate = 10:1).

*2.2.2. General procedure for the cross-coupling of 4,7-dibromobenzo[c][1,2,5]chalcogenadiazoles **5** and boronic ester **4**.*

In 50 ml round-bottom flask, **4** (450 mg, 1.2 mmol) and 4,7-dibromobenzo-1,2,5-chalcogenadiazole **5** (1.2 mmol) were dissolved in 15 ml of dioxane, and 2 M K_2CO_3 (10 ml) was added. The mixture was degassed for 20 minutes with a stream of argon, after which time $Pd(PPh_3)_4$ (67 mg, 60 µmol, 5%) was added. After refluxing for 10 h, the mixture was extracted with ethylacetate; organic solvent was then removed under reduced pressure. The residue was purified on a silica gel column with eluent ethylacetate/petroleum ether = 1:25.

4-Bromo-7-(9-(p-tolyl)-2,3,4,4a,9,9a-hexahydro-1H-carbazol-6-yl)benzo[c][1,2,5]thiadiazole (***6a***)

Orange solid with mp 127-129 ºC (330 mg, 58%). ^{1}H NMR (300 MHz, δ, ppm): 7.88 (d, J=7.6 Hz, 1H), 7.73 (s, 1H), 7.65 (d, J=8.3 Hz, 1H), 7.52 (d, J=7.7 Hz, 1H), 7.22 (m, 4H), 6.86 (d, J=8.3 Hz, 1H), 4.17 (m, 1H), 3.35 (m, 1H), 2.39 (s, 3H), 1.97-1.87 (m, 1H), 1.84-1.72 (m, 3H), 1.62-1.41 (m, 4H). ^{13}C NMR (75 MHz, δ, ppm): 154.1, 153.5, 150.1, 140.3, 135.5, 134.8, 133.7, 132.5 130.0, 128.7, 126.9, 126.7, 124.2, 123.2, 111.1, 108.8, 64.8, 40.6, 28.3, 25.9, 22.8, 21.2, 21.0. HRMS-ESI (m/z): $[M+H]^+$ calcd for ($C_{25}H_{22}BrN_3S$) 476.0791, found 476.0792. UV-Vis (CH_2Cl_2, λ_{max}, nm/logε): 276/4.38, 415/3.83. IR, ν, cm^{-1}: 2923, 2852, 1605, 1513, 1466, 1377, 1328, 1256, 883, 807, 506. R_f = 0.37 (15 petroleum ether/1 ethylacetate).

4-Bromo-7-(9-(p-tolyl)-2,3,4,4a,9,9a-hexahydro-1H-carbazol-6-yl)benzo[c][1,2,5]oxadiazole (***6b***)

Orange solid with mp 142-144 ºC (328 mg, 65%). ^{1}H NMR (300 MHz, δ, ppm): 7.80 (s, 1H), 7.73 (d, J=8.4 Hz, 1H), 7.64 (d, J=7.5 Hz, 1H), 7.35 (d, J=7.5 Hz, 1H), 7.22 (q, J=8.5 Hz, 4H), 6.82 (d, J=8.3 Hz, 1H), 4.18 (m, 1H), 3.34 (m, 1H), 2.40 (s, 3H), 1.98-1.88 (m, 1H), 1.84-1.72 (m, 3H), 1.62-1.41 (m, 4H). ^{13}C NMR (75 MHz, δ, ppm): 150.9, 150.2, 149.0, 139.9, 135.8, 134.7, 134.0, 130.1, 128.2, 125.8, 124.8, 123.4, 112.1, 108.9, 104.8, 64.9, 40.5, 28.2, 25.9, 22.7, 21.2, 21.1. HRMS-ESI (m/z): $[M+H]^+$ calcd for ($C_{25}H_{22}BrN_3O$) 462.1000, found 462.0989. UV-Vis (CH_2Cl_2, λ_{max}, nm/logε): 310/4.21, 480/4. IR, ν, cm^{-1}: 2925, 2853, 1606, 1514, 1482, 1380, 1269, 806. R_f=0,46 (10 petroleum ether/1 ethylacetate).

4-Bromo-7-(9-(p-tolyl)-2,3,4,4a,9,9a-hexahydro-1H-carbazol-6-yl)benzo[c][1,2,5]selenadiazole (***6c***)

Orange solid with mp 178-180 ºC (410 mg, 65%) ^{1}H NMR (300 MHz, δ, ppm): 7.80 (d, J=7.5 Hz, 1H), 7.64 (s, 1H), 7.57 (d, J=8.2 Hz, 1H), 7.35 (d, J=7.5 Hz, 1H), 7.22 (m, 4H), 6.85 (d, J=8.2 Hz, 1H), 4.17 (m, 1H), 3.34 (m, 1H), 2.39 (s, 3H), 1.93-1.71 (m, 4H), 1.63-1.53 (m, 2H), 1.47-1.39 (m, 2H). ^{13}C NMR (75 MHz, δ, ppm): 158.8, 158.7, 149.9, 140.3, 136.4, 135.2, 133.5, 132.5, 129.9, 128.9, 127.5, 126.7, 124.4, 123.1, 113.8, 108.6, 64.7, 40.5, 28.2, 25.8, 22.8, 21.1, 20.9. HRMS-ESI (m/z): $[M+H]^+$ calcd for ($C_{25}H_{22}BrN_3Se$) 524.0234, found 524.0224. UV-Vis (CH_2Cl_2, λ_{max}, nm/logε): 323/4.56, 495/3.99. IR, ν, cm^{-1}: 2927, 2853, 1605, 1513, 1481, 1380, 1268, 806. R_f=0,58 (5 petroleum ether/1 ethylacetate).

*2.2.3. General procedure for the cross-coupling reaction of mono-adducts **6a-c** and tert-butyl 2-cyano-3-(5-(4,4,5,5-tetramethyl-1,3,2-dioxaborolan-2-yl)thiophen-2-yl)acrylate **7**.*

In 50 ml round-bottom flask, mono-adduct **6a-c** (0.45 mmol) and ester **7** (220 mg, 0.61 mmol) were dissolved in 10 ml of dioxane, and then 2M K_2CO_3 (10 ml) was added. The mixture was

degassed for 20 minutes with a stream of argon, $Pd(PPh_3)_4$ (30 mg, 26 μmol, 5%) was added. After refluxing for 12 h, the mixture was extracted with ethylacetate and solvent was removed under reduced pressure. The residue was purified on a silica gel column with eluent ethylacetate/petroleum ether = 1:20.

tert-Butyl 2-cyano-3-(5-(7-(9-(p-tolyl)-2,3,4,4a,9,9a-hexahydro-1H-carbazol-6-yl)benzo[c][1,2,5]thiadiazol-4-yl)thiophen-2-yl)acrylate ***8a****.*

Dark red solid with mp 194-196 ºC (135 mg, 41%). ^{1}H NMR (300 MHz, δ, ppm): 8.28 (s, 1H), 8.26 (d, J=4.2 Hz, 1H), 8.06 (d, J=7.6 Hz, 1H), 7.89 (d, J=4.1 Hz, 1H), 7.82 (s, 1H), 7.76 (d, J=8.6 Hz, 1H) 7.71 (d, J=7.6 Hz, 1H), 7.23 (s, 4H), 6.87 (d, J=8.3 Hz, 1H), 4.19 (m,1H), 3.36 (m, 1H), 2.39 (s, 3H), 1.97-1.90 (s, 1H) 1.85-1.75 (m, 3H), 1.62 (s, 9H), 1.58-1.40 (m, 4H). ^{13}C NMR (75 MHz, δ, ppm): 161.8, 154.0, 152.7, 150.2, 149.1, 145.4, 140.1, 137.8, 135.8, 135.4, 133.6, 129.9, 129.0, 128.0, 127.9, 127.0, 125.9, 124.2, 123.2, 123.0, 116.3, 108.7, 100.1, 83.4, 64.8, 40.5, 28.2, 28.0, 25.8, 22.7, 21.1, 20.9. HRMS-ESI (m/z): $[M]^+$calcd for ($C_{37}H_{34}N_4O_2S_2$) 630.2118 , found 630.2112. UV-Vis (CH_2Cl_2, λ_{max}, nm/logε): 318/4.41, 414/4.31, 523/4.44. IR, ν, cm^{-1}: 2931, 2855, 2180, 1709, 1605, 1585, 1510, 1458, 1363, 1248, 1152, 808. R_f = 0.44 (petroleum ether/ ethylacetate = 5:1).

tert-Butyl 2-cyano-3-(5-(7-(9-(p-tolyl)-2,3,4,4a,9,9a-hexahydro-1H-carbazol-6-yl)benzo[c][1,2,5]oxadiazol-4-yl)thiophen-2-yl)acrylate ***8b****.*

Dark purple solid with mp 120-122 ºC (127 mg, 46%). ^{1}H NMR (300 MHz, δ, ppm): 8.27 (s, 1H), 8.24 (d, J=4.1 Hz, 1H), 7.90 (s, 1H), 7.83 (m, 3H), 7.57 (d, J=7.5 Hz, 1H), 7.23 (q, J=8.5 Hz, 4H), 6.85 (d, J=8.3 Hz, 1H), 4.19 (m, 1H), 3.37 (m, 1H), 2.40 (s, 3H), 1.97-1.90 (s, 1H) 1.85-1.75 (m, 3H), 1.62 (s, 9H), 1.58-1.40 (m, 4H). ^{13}C NMR (75 MHz, δ, ppm): 161.5, 151.0, 149.0, 148.0, 147.2, 145.2, 139.7, 138.7, 135.7, 135.7, 134.0, 131.3, 130.0, 129.4, 128.9, 128.5, 125.1, 124.9, 123.3, 118.6, 116.1, 108.8, 100.8, 83.6, 64.9, 40.3, 28.1, 28.0, 25.8, 22.6, 21.0, 21.0. HRMS-ESI (m/z): $[M+H]^+$ calcd for ($C_{37}H_{34}N_4O_3S$) 615.2424, found 615.2411; $[M+Na]^+$ calcd for ($C_{37}H_{34}N_4O_3SNa$) 637.2244, found 637.2245. UV-Vis (CH_2Cl_2, λ_{max}, nm/logε): 310/4.30, 405/4.18, 550/4.41. IR, ν, cm^{-1}: 2927, 2854, 2216, 1702, 1605, 1578, 1513, 1482, 1370, 1268, 807, 654. R_f = 0.52 (petroleum ether/ ethylacetate = 5:1).

tert-Butyl 2-cyano-3-(5-(7-(9-(p-tolyl)-2,3,4,4a,9,9a-hexahydro-1H-carbazol-6-yl)benzo[c][1,2,5]selenadiazol-4-yl)thiophen-2-yl)acrylate ***8c****.*

Dark purple solid with mp 98-100 ºC (192 mg, 49%). ^{1}H NMR (300 MHz, δ, ppm): 8.28 (s, 1H), 8.15 (d, J=4.1 Hz, 1H), 8.00 (d, J=7.5 Hz, 1H), 7.91 (d, J=4.1 Hz, 1H), 7.74 (s, 1H), 7.67 (d, J=8.3 Hz, 1H), 7.58 (d, J=7.5 Hz, 1H), 7.22 (s, 4H), 6.86 (d, J=8.3 Hz, 1H), 4.18 (m, 1H),

3.36 (m, 1H), 2.40 (s, 3H), 1.97-1.88 (s, 1H) 1.84-1.72 (m, 3H), 1.61 (s, 9H), 1.58-1.40 (m, 4H). ^{13}C NMR (75 MHz, δ, ppm): 162.0, 159.7, 158.3, 150.2, 149.6, 145.7, 140.3, 137.5, 137.4, 136.7, 135.3, 133.7, 130.0, 129.3, 128.4, 127.9, 126.3, 124.8, 124.6, 123.2, 116.5, 108.7, 99.9, 83.5, 64.8, 40.6, 28.3, 28.1, 25.9, 22.7, 21.2, 21.0. HRMS-ESI (m/z): $[M+H]^+$ calcd for ($C_{37}H_{34}N_4O_2SSe$) 679.1643, found 679.1628. UV-Vis (CH_2Cl_2, λ_{max}, nm/logε): 326/4.57, 405/4.33, 550/4.55. IR, ν, cm^{-1}: 2929, 2853, 2215, 1719, 1601, 1511, 1470, 1370, 1278, 1160, 840, 733. R_f = 0.38 (petroleum ether/ ethylacetate = 5:1).

2.2.4. General procedure for hydrolyses of ethers **8a-c**.

In a 25 ml round-bottom flask, **8a-c** (0.15 mmol, 96 mg, 92 mg and 104 mg respectively) was dissolved in a 5 ml solution of 1/3 $CF_3COOH/CHCl_3$. After stirring for 4 h under argon, the mixture was diluted with dichloromethane, washed with water, and removed under reduced pressure. The residue was purified on a silica gel column with eluent methanol/dichloromethane/acetic acid = 10:50:1.

2-Cyano-3-(5-(7-(9-(p-tolyl)-2,3,4,4a,9,9a-hexahydro-1H-carbazol-6-yl)benzo[c][1,2,5]thiadiazol-4-yl)thiophen-2-yl)acrylic acid (***MAX114***)

Dark red solid with mp >300 ºC (79 mg, 91%). ^{1}H NMR (300 MHz, DMSO-d6, δ, ppm): 8.19 (m,2H), 8.10 (s, 1H), 7.88 (s, 1H), 7.85 (d, J=7.7 Hz, 1H), 7.79 (m, 2H), 7.23 (m, 4H), 6.80 (d, J=8.3 Hz, 1H), 4.21 (m, 1H), 2.32 (s, 3H), 1.90-1.82 (m, 1H) 1.74-1.59 (m, 3H), 1.47-1.33 (m, 4H). ^{13}C NMR (75 MHz, DMSO-d_6, δ, ppm): 162.9, 153.6, 152.5, 149.5, 143.5, 140.2, 139.9, 138.7, 135.4, 135.1, 133.9, 133.2, 130.4, 129.2, 127.7, 127.6, 127.3, 126.7, 124.5, 123.5, 122.8, 120.0, 111.5, 108.6, 64.2, 27.9, 25.7, 22.5, 21.1, 21.0. MS-MALDI (m/z): $[M]^+$ calcd for ($C_{33}H_{26}N_4O_2S_2$) 574.1497, found 574.2726. UV-Vis (CH_2Cl_2/MeOH (2%), λ_{max}, nm/logε): 365/4.10, 482/4.19. IR, ν, cm^{-1}: 2924, 2853, 2211, 1720, 1610, 1578, 1515, 1474, 1377, 1268, 806. R_f = 0.47 (ethylacetate/ methanol = 2:1).

2-Cyano-3-(5-(7-(9-(p-tolyl)-2,3,4,4a,9,9a-hexahydro-1H-carbazol-6-yl)benzo[c][1,2,5]selenadiazol-4-yl)thiophen-2-yl)acrylic acid (***MAX115***)

Dark purple solid with mp >300 ºC (83 mg, 88%). ^{1}H NMR (300 MHz, DMSO-d6, δ, ppm): 8.13 (d, J=4.1 Hz, 1H), 8.08 (m, 2H), 7.81 (s, 1H), 7.77 (d, J=4.1 Hz, 1H), 7.68 (m, 2H), 7.23 (m, 4H), 6.78 (d, J=8.4 Hz, 1H), 4.20 (m, 1H), 2.32 (s, 3H), 1.90-1.82 (m, 1H) 1.74-1.59 (m, 3H), 1.47-1.33 (m, 4H). ^{13}C NMR (75 MHz, DMSO-d6, δ, ppm): 163.3, 158.5, 157.32, 148.7, 144.0, 140.0, 139.8, 138.1, 135.2, 134.5, 134.2, 132.5, 129.9, 129.0, 127.8, 127.2, 127.0, 126.0, 124.7, 124.4, 122.2, 119.4, 109.9, 107.9, 63.7, 27.4, 25.2, 22.0, 20.6, 20.4. MS-MALDI (m/z): $[M]^+$ calcd for ($C_{33}H_{26}N_4O_2SSe$) 622.0944, found 622.2408. UV-Vis (CH_2Cl_2/MeOH (2%),

λ_{max}, nm/logε): 375/4.14, 512/4.12. IR, ν, cm^{-1}: 2924, 2853, 2214, 1718, 1604, 1582, 1511, 1466, 1378, 1271, 1151, 809. R_f = 0.49 (ethylacetate/ methanol = 2:1).

2-Cyano-3-(5-(7-(9-(p-tolyl)-2,3,4,4a,9,9a-hexahydro-1H-carbazol-6-yl)benzo[c][1,2,5]oxadiazol-4-yl)thiophen-2-yl)acrylic acid (***MAX123***)

Dark purple solid with mp >300 ºC (77 mg, 92%). ^{1}H NMR (300 MHz, DMSO-d6, δ, ppm): 8.17 (s, 1H), 8.06 (d, J=3.9 Hz, 1H), 7.94 (d, J=7.5 Hz, 1H), 7.88 (s, 1H), 7.81 (m, 2H), 7.75 (d, J=7.6 Hz, 1H), 7.21 (q, J=8.4 Hz, 4H), 6.77 (d, J=8.4 Hz, 1H), 4.21 (m, 1H), 2.32 (s, 3H), 1.91-1.82 (m, 1H) 1.74-1.64 (m, 2H), 1.62-1.53 (m, 1H), 1.47-1.33 (m, 4H). ^{13}C NMR (75 MHz, DMSO-d6, δ, ppm): 164.5, 150.1, 148.9, 148.0, 142.8, 141.3, 140.0, 138.1, 136.5, 135.7, 133.4, 130.4, 129.6, 129.2, 128.6, 128.2, 126.6, 124.9, 123.3, 122.8, 119.2, 118.4, 109.4, 108.6, 64.2, 27.8, 25.6, 22.4, 21.0. MS-MALDI (m/z): $[M]^+$ calcd for ($C_{33}H_{26}N_4O_3S$) 558.1725, found 558.2721. UV-Vis (CH_2Cl_2/MeOH (2%), λ_{max}, nm/logε): 367/3.66, 506/3.85. IR, ν, cm^{-1}: 2930, 2855, 2214, 1715, 1586, 1512, 1482, 1370, 1266, 1153, 808. R_f = 0.51 (ethylacetate/ methanol = 2:1).

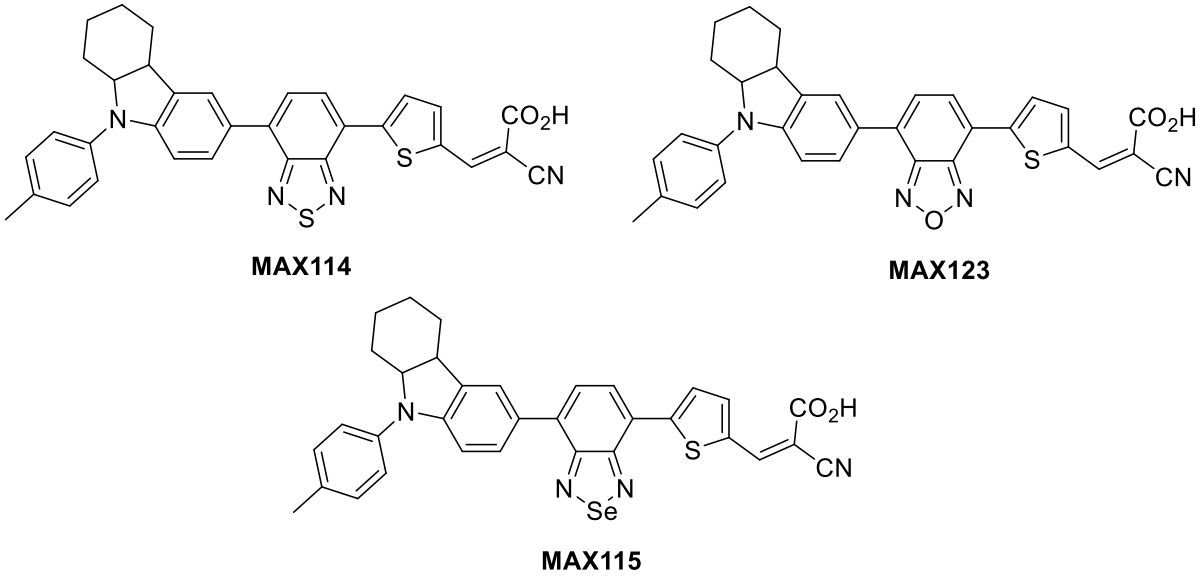

Scheme 1. Chemical structures of **MAX114**, **MAX123** and **MAX115**.

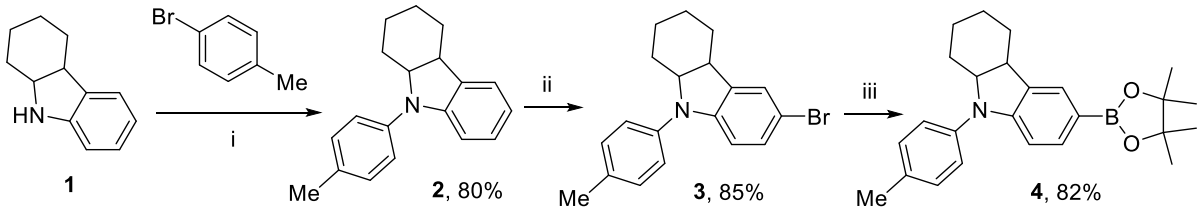

Scheme 2. Synthesis of new donor building block **1**. The reaction conditions: (i) $Pd(OAc)_2$, $PtBu_3$, Cs_2CO_3, xylene; (ii) HBr, DMSO, ethylacetate (iii) B_2Pin_2, KOAc, Pd_2dba_3, X-Phos, dioxane.

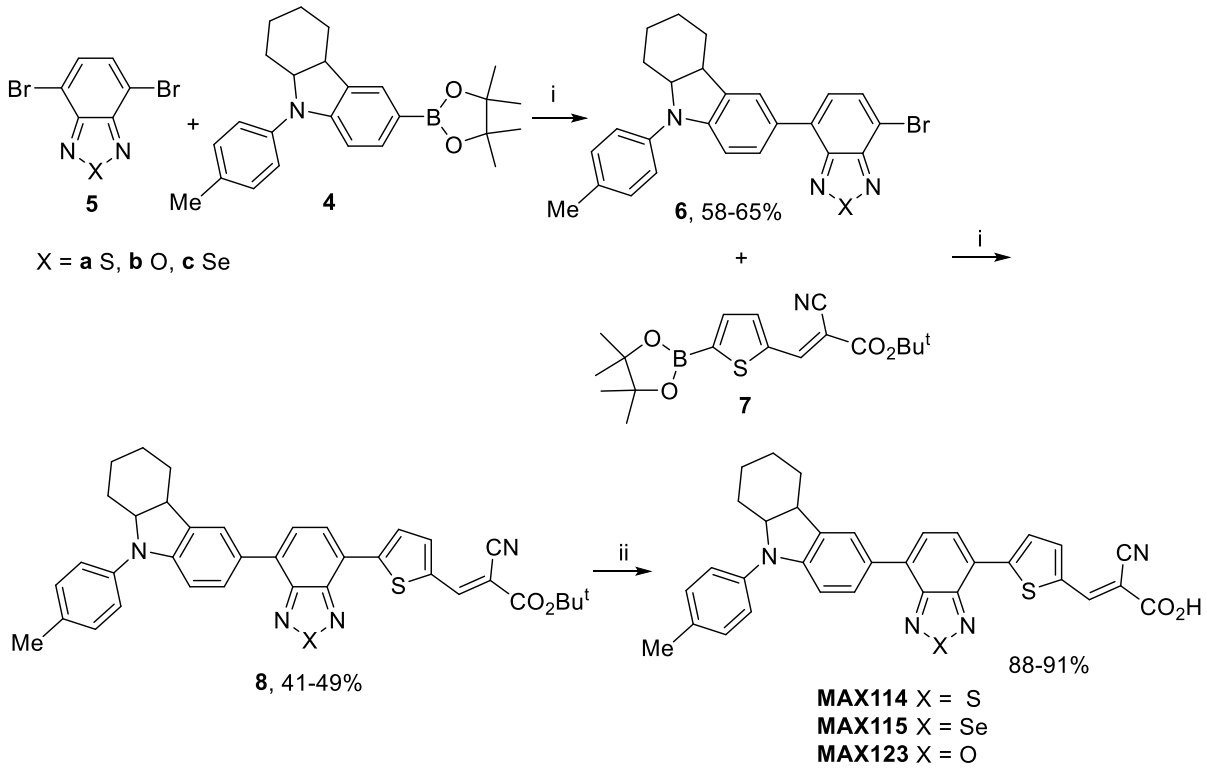

Scheme 3. Synthesis of sensitizers. The reaction conditions: (i) $Pd(PPh_3)_4$, K_2CO_3, dioxane; (ii) CF_3COOH, $CHCl_3$

3. Results and Discussion

3.1 Synthesis and characterization

The molecular structures of the dyes, containing the novel donor building-block - 9-(*p*-tolyl)-2,3,4,4a,9,9a-hexahydro-1*H*-carbazole, are shown in Scheme 1. 4,6-(4,4,5,5-Tetramethyl-1,3,2-dioxaborolan-2-yl)-9-(p-tolyl)-1,2,3,4,4a,9a-hexahydrocarbazole **4** was prepared in four steps from 1,2,3,4,4a,9a-hexahydrocarbazole **1** Scheme 2. Buchwald-Hartwig arylation of hexahydrocarbazole with *p*-iodotoluene in the presence of $Pd(OAc)_2$, P^tBu_3 and Cs_2CO_3 in xylene afforded the *p*-tolyl derivative in good yield (80%). Bromination of the aromatic ring with a mixture of HBr and DMSO followed by Miayura borylation with 4,4,4',4',5,5,5',5'-octamethyl-2,2'-bi(1,3,2-dioxaborolane) in the presence of palladium catalyst Pd_2dba_3, ligand X-Phos and KOAc in 1,4-dioxane gave key the donor component in good yield.

The general strategy for the synthesis of dyes with D-A^1-π-A^2 motif follows a stepwise approach shown in Scheme 3. Internal acceptors A^1 - 4,7-dibromobenzo[*c*][1,2,5]thiadiazole **5a** [41], 4,7-dibromobenzo[*c*][1,2,5]oxadiazole **5b** [42] 4,7-dibromobenzo[*c*][1,2,5]selenadiazole **5b** [43] and π-spacer-acceptor moiety - *tert*-butyl (2-cyano-3-(5-(4,4,5,5-tetramethyl-1,3,2-dioxaborolan-2-yl)thiophen-2-yl)acrylate [44] were prepared by known procedures. The cross-coupling reactions of 4,7-dibromobenzo[*c*][1,2,5]chalcogenadiazoles (**5**) with donor boronic ester **4** in the presence of $Pd(PPh_3)_4$ as a catalyst and aqueous solution K_2CO_3 in THF successfully gave mono-adducts **6a-c** in moderate yields. The second cross-coupling of 7-bromobenzo[*c*][1,2,5]chalcogenadiazoles **6a-c** with acceptor *tert*-butyl ester gave bis-adducts **8a-c** in high yields. Final hydrolysis of compounds **8a-c** with CF_3CO_2H resulted in the formation of the target **MAX** dyes in high yields. All dyes were purified by column chromatography before measurement of the physical and electrochemical properties as well as solar cell device fabrication.

3.2 Photophysical and electrochemical properties

The response region in sunlight for DSSCs is determined primarily by the UV-Vis absorption of the sensitizer. Therefore, we initially characterized the spectral response of the **MAX** series in DCM/MeOH (V/V = 98/2) at 4×10^{-5} mol L^{-1} (Fig. 1). The absorption peaks (λ_{max}) and their corresponding molar absorption coefficients (ε) are listed in Table 1. As shown in Fig. 1, all these dyes exhibit two absorption regions. The absorption peaks between 350-400 nm mainly correspond to the π-π* electron transition. The broad absorption bands in the 450-550 nm region are assigned to an intramolecular charge transfer (ICT) process between the donor and anchor/acceptor group, which produces the efficient charge-separated excited state. Despite the fact that the extinction coefficient of the sulfur-containing derivative **MAX114** is as close as possible to the same value of the previously-described **WS-2** dye (15.5×10^3 $M^{-1}\cdot cm^{-1}$ and 16.7×10^3 $M^{-1}\cdot cm^{-1}$, correspondingly) [16]), the second absorption band suffers strong hypsochromic shift from λ_{max} = 533 nm for **WS-2** to 482 nm for **MAX114**. Thus, a small change in the donor fragment (addition of one CH_2 group in the indoline ring) has a significant effect on the second absorption maximum, which indicates a high sensitivity of intramolecular electron transfer to even small variations in the structure of the donor part of the molecules. We found that the nature of the chalcogen in the internal acceptor affects the long-wave absorption maximum. **MAX** dyes show a significant bathochromic shift during the replacement

of the sulfur atom in the 1,2,5-chalcogenadiazole ring on the more electronegative oxygen atom (24 nm), and the more electropositive atom of selenium (30 nm). At the same time, the short-wave absorption maximum (about 370 nm) is practically independent of the chalcogen atom in the heterocycle: the deviation is no more than 10 nm. Probably, such a nonlinear dependence can be explained, on the one hand, by a decrease in the electronegativity of sulfur in comparison with oxygen, which reduces the efficiency of intramolecular charge transfer by reducing the electron acceptor effect of the chalcogenadiazole fragment. On the other hand, an increase in the radius of the atom in the transition from sulfur to selenium seems to contribute to the ICT process due to the presence of d-orbitals in the selenium atom that can participate in the conjugation. The extinction coefficient was also dependent on the nature of the chalcogen: the smallest extinction was observed for the oxygen-containing compound **MAX123** (6.8×10^3 $M^{-1} \cdot cm^{-1}$). However, in this case, the dye based on thiadiazole showed values that do not correspond to the linear change in the sequential change of chalcogen atoms: the extinction coefficient for the sulfur-containing dye (**MAX114**) was 15.5×10^3 $M^{-1} \cdot cm^{-1}$, while the selenium analogue (**MAX115**) showed a value of 13.0×10^3 $M^{-1} \cdot cm^{-1}$. Thus, the maximum conjugation has dyes based on sulfur and selenium, and the introduction of an electronegative oxygen atom with a minimum radius probably alters the geometry of the molecule, reducing the conjugation. The calculated $E_{g\ opt}$ for known dye **WS-2** is much less compared to the dyes of the **MAX** series. It is surprising that the oxygen and selenium dyes (**MAX115** and **MAX123**) showed better results, compared with the sulfur-containing compound **MAX114**, which is the closest analog of **WS-2** (Table 1).

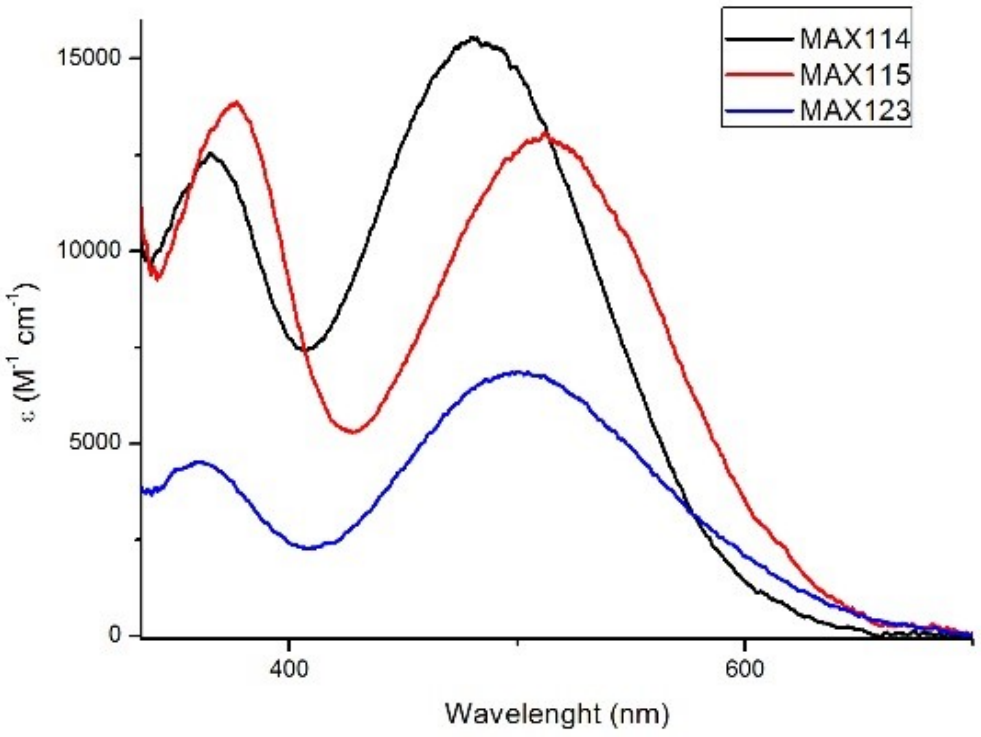

Fig. 1 UV-Visible absorption (a) in DCM/MeOH (V/V = 98/2) at 4×10^{-5} mol L^{-1} of **MAX** dyes.

Table 1. UV-Visible absorption properties of the **MAX** series in DCM/MeOH (V/V = 98/2) solutions.

Dye	λ_{max1}, [nm][a]	$\varepsilon_{max1} \times 10^3$, [$M^{-1}\cdot cm^{-1}$][a]	λ_{max2}, [nm][a]	$\varepsilon_{max2} \times 10^3$, [$M^{-1}\cdot cm^{-1}$][a]	λ_{onset}, [nm][a]	$E_{g,\,opt}$, eV[b]
MAX114	365	12.5	482	15.5	595	2.087
MAX115	375	13.8	512	13.0	629	1.975
MAX123	367	4.4	506	6.8	633	1.962
WS-2 [c]			533	16.7	675	1.840

[a] Absorption peaks (λ_{max}, λ_{onset}) and molar extinction coefficients (ε) in DCM/MeOH (V/V = 98/2) [b] Calculated by $1242/\lambda_{onset}$ [c] [16]

To estimate the energy value of the frontier orbitals, the potential values of the first oxidation and reduction peaks on the cyclic voltammetry curves of the investigated compounds in DMF were obtained. Figure 2 shows a cyclic voltammogram of the new sensitizers obtained

versus ferrocene/ferrocenium (Fc/Fc+) at a scan rate of 100 mVs^{-1}. Electroreduction peaks, as seen in Fig.1, are reversible at low potential sweep rates. Electrooxidation of all compounds is irreversible even at a sweep rate of 10 Vs^{-1}. Relevant electrochemical data for the compounds are presented in Table 2. Assuming a value of -5.1 eV [45,46] for the absolute potential of the Fc/Fc+ couple in non-aqueous electrolytes, E_{HOMO} and E_{LUMO} were calculated using equations (1) and (2):

$$E_{HOMO}\ (eV) = -\ |e|(E^{ox}{}_{Fc/Fc+} + 5.1) \quad (1)$$
$$E_{LUMO}\ (eV) = -\ |e|(E^{red}{}_{Fc/Fc+} + 5.1) \quad (2)$$

As a result, E_{LUMO} of **MAX114** (-3.48 eV), **MAX115** (-3.57 eV) and **MAX123** (-3.63 eV) are higher in energy than the conduction band edge of nanocrystalline TiO_2 (-4.2 eV) [47], indicating that the electron injection process from the excited dye molecules to the TiO_2 conduction band is energetically permitted. However, in the series of three dyes, there is no linear dependence of these values in the transition from an oxygen-containing analogue **MAX115** to a selenium-containing one **MAX123**. The minimum value of E_{LUMO}, is seen for the dye based on thiadiazole **MAX114**. Since the energy of the LUMO depends on the degree of conjugation of the molecule [48,49], it can be assumed that an increase in the electronegativity of the central chalcogen atom by transition from thiadiazole to oxadiazole leads to too strong charge separation, while the transition to a more voluminous selenium atom leads to a reduction in conjugation due to an increase in the radius of the central atom and changes in the geometry of the molecule.

The E_{HOMO} level of **MAX114** (-5.39 eV), **MAX115** (-5.34 eV) and **MAX123** (-5.44 eV) show more negative values than the energy level of I^-/I_3^- redox (-5.2 eV) [50], therefore, dye regeneration should be thermodynamically favorable. Since the HOMO energy is dependent mostly on the nature of the donor fragment of the molecules, it is not surprising that the values of E_{HOMO} for all three dyes differ by no more than 0.1 eV.

Comparison of the E_{LUMO} level of **MAX114** with the corresponding values of the known analogue **WS-2** (Table 2, [52]), differing in the size of the alicycle in the donor part of the molecule, leads to the conclusion that the replacement of the cyclopentane fragment in the donor in **WS-2** to cyclohexane in **MAX114**, apparently leads to a decrease in the degree of conjugation of the molecule. The decrease in the E_{HOMO} level of **MAX114** compared to **WS-2** by 0.38 eV indicates an increase in the degree of delocalization of the donor fragment containing the cyclohexane ring.

The electrochemical gap energy E_g^{CV} for each dye is calculated from the difference between their E_{HOMO} and E_{LUMO}. All E_g values (Table 2) satisfy the design expectation that this value for dye-sensitized solar cells should be less than 2.5 eV [51]. As a result, all dyes have enough energetic driving force for efficient DSSCs using a nanocrystalline titania photocatalyst and the I^-/I_3^- redox couple.

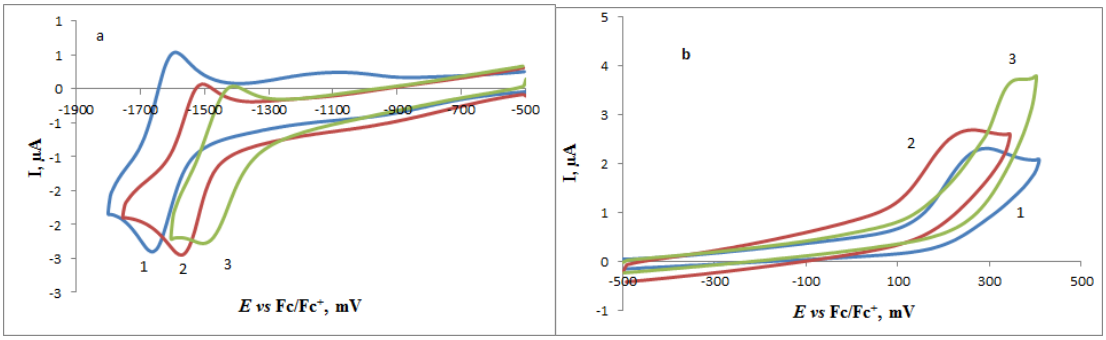

(a) (b)

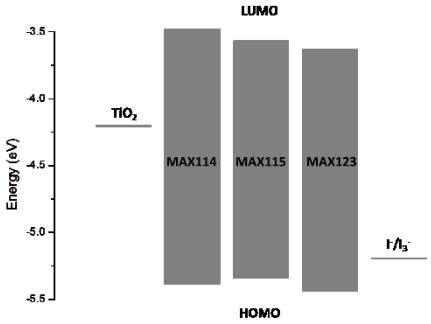

(c)

Fig. 2. Cyclic voltammogram showing reduction (a) and oxidation (b) of **MAX 114** (1), **MAX 115** (2), **MAX 123** (3). Scan rate 100 mVs^{-1}, electrolyte 0.1 M Bu_4NClO_4 in DMF. (c) Schematic diagram of energy levels of TiO_2 conduction band, dyes and I^-/I_3^- redox couple.

Table 2. Electrochemical properties of the dyes in DMF solutions.

Compound	E^{red} (*vs* Fc/Fc^+)[a], V	E_{LUMO}[b], eV	E^{ox} (*vs* Fc/Fc^+)[a], V	E_{HOMO}[b], eV	E_g[c], eV
MAX 114	-1.62	-3.48	0.29	-5.39	1.91
MAX 115	-1.53	-3.57	0.24	-5.34	1.77
MAX 123	-1.47	-3.63	0.34	-5.44	1.80

WS-2	-1.33[d]	-3.77	0.67[d]	-5.77	2.00[52]

[a] Here E^{ox}_{onset} and E^{red}_{onset} are oxidation and reduction peak potential relative to Fc/Fc^{+} respectively

[b] Energies of frontier orbitals were calculated according to equations (1) and (2)

[c] $Eg = E_{LUMO} - E_{HOMO}$

Unsurprisingly the E_g data of the **MAX** dyes obtained from the CV data agree well with the absorption onset. Thiadiazole dye (**MAX114**) has a bit higher E_g than its selenium and oxygen counterparts. This enhancement can lead apparently to a longer lifetime of the first excited state of **MAX114**, which should have a positive impact on the photovoltaic efficiency of solar cells made on its basis. These data once again prove the better photovoltaic properties of fused thiadiazoles compared to oxa - and selenadiazole analogs, which leads to nonlinear changes in the properties of a number of chalcogen atoms. The E_g value for the known dye **WS-2** is close to its structural analogue **MAX114**, which should lead to close parameters of solar cells based on these compounds.

3.3 DSC performance

To study the influence of the chalcogen atom in chalcogenadiazole ring of the central acceptor unit of the dye on the photovoltaic efficiency, we constructed DSSCs based on the dye series **MAX**. Commercially available ruthenium dye **N719** was chosen as a reference dye. The J-V curves are shown on Fig. 3 and the results are summarized in Table 3. Fill factors (FF) have similar values for all dyes in the **MAX** series, from 0.61 to 0.64, therefore PCE values will depend mainly on open-circuit voltage (V_{oc}) and short-circuit current density (J_{sc}). V_{oc} values for all three dyes of the **MAX** series are approximately equal to each other~~. There are two main factors that result in the variation of V_{oc}. The first is the quasi-Fermi level shift and the second is recombination of injected electrons with oxidized sensitizer or electrolyte.~~ The three dyes possess similar structures such that suppression of electronic recombination is likely to be similar in each case. To confirm this, the electron lifetime of the conduction band electrons in the TiO_2 (= electron lifetime) was analyzed by electrochemical impedance spectroscopy. Fig. S4 shows the electron lifetime plot against V_{OC} with the **MAX** DSSCs. The values were derived from the peak frequency in the Bode plots. In comparison with the reference **N719**, the electron lifetime trends are similar among the series, ranging around 2-5 ms at 0.8-1.0 sun. The results are coherent with the similar V_{OC} values achieved by the three dyes. ~~Accordingly, the primary factor for the voltage is more likely to be the quasi-Fermi level shift due to the different amount of injected electrons from the excited dyes into the conduction band of TiO_2 with various LUMO levels.~~

The J_{sc} of the benzothiadiazole dye **MAX114** issignificantly higher than the oxygen analogue **MAX123**. The selenadiazole **MAX115** sits between MAX114 and MAX123. This is consistent with the fact that the dye **MAX114** has the highest extinction coefficient but is contrary to the values of long-wavelength absorption maxima. Since all three dyes have similar HOMO values (the difference does not exceed 0.1 eV), it is likely that the oxidized state, formed after electron injection, in all three dyes is easily regenerated to the neutral state. The interesting fact is that the values of LUMO energy level of synthesized dyes change nonlinearly when moving from oxygen-containing **MAX123** through sulfur- (**MAX114**) to selenium-analogues (**MAX115**). Thiadiazole derivative **MAX114** has the higher LUMO level whilst the values of LUMO energy level of **MAX115** and **MAX123** are, respectively, 0.09 and 0.15 eV lower. The energy gap values of **MAX115** and **MAX123** dyes obtained by cyclic voltammetry are 0.14 and 0.11 eV, respectively, less than the E_g of the **MAX114** dye. The energy gap values obtained from the optical data are consistent with the E_g^{CV} values: the difference between the values exceeded 0.1 eV. The combination of these factors leads to relatively low values of the photovoltaic efficiency of oxygen-containing dye in comparison with the sulfur and shows that the performance of sulfur-based dyes should be superior than oxygen and selenium-based dyes.

The dark current in DSSCs based on **N719** dyeis less than that for the **MAX** series dyes, which means less effective suppression of charge recombination from TiO_2 to the electrolyte for the latter.

It is interesting to note that the current-voltage characteristics for DSSCs based on the dye **WS-2**, performed under similar conditions [52], are lower than the similar dye **MAX114**, differing by one CH_2 group in the donor alicyclic fragment. The most important difference for **WS-2** and **MAX114** was found for J_{sc} and consequently for PCE; 5.07 and 5.86%, respectively. The incident photon-to-current efficiency curves (Fig. S25) also support the superior J_{SC} of MAX114 to WS-2. Unlike the UV-Visible absorption in solution (Fig. 1), the optical absorption of MAX114 is efficient throughout the visible spectrum. The poorer results for MAX115 and MAX123 are consistent with our predictions above.

Table 3. *J-V* characteristics for DSSCs based on the dyes **MAX** series and **N719**[a].

Dye	V_{oc} (mV)	J_{sc} (mA cm^{-2})	FF	η (%)
MAX114	0.64	14.75	0.62	5.86
MAX115	0.65	13.75	0.64	5.78
MAX123	0.64	11.90	0.61	4.66
N719	0.78	15.32	0.63	7.54
WS-2	0.59	11.8	0.63	5.07

[a] The data given for MAX dyes and N719 were obtained with 8 μm (4 μm transparent + 4 μm scattering) TiO_2 films and CDCA additive. The data for WS2 was taken from the paper [52] and were obtained with 12 μm (8 μm transparent + 4 μm scattering) TiO_2 films and no CDCA additive.

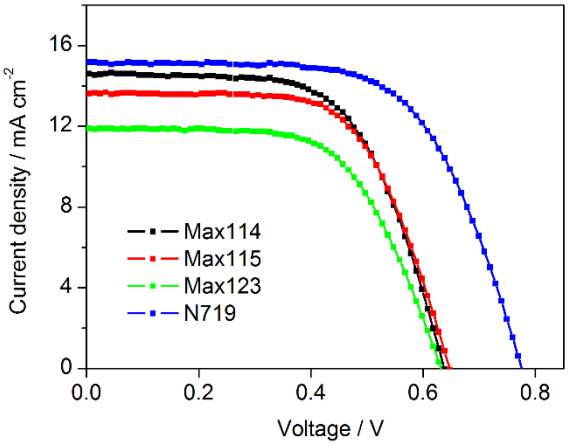

Fig. 3. *J-V* characteristic for DSSCs based on the dyes **MAX** series and **N719**

4 Conclusions

In summary, we have synthesized 4,6-(4,4,5,5-tetramethyl-1,3,2-dioxaborolan-2-yl)-9-(p-tolyl)-1,2,3,4,4a,9a-hexahydrocarbazole - a new donor building-block for DSSCs. Three novel D-A-π-A metal-free organic sensitizers were obtained using this donor. 2,1,3-Benzothiadiazole sensitizer **MAX114** based on 9-(*p*-tolyl)-2,3,4,4a,9,9a-hexahydro-1*H*-carbazole showed higher PCE by comparison to the well-known 4-(*p*-tolyl)-1,2,3,3a,4,8b-hexahydrocyclopenta[*b*]indolyl building block, which is varied from extensively investigated 4-(*p*-tolyl)-1,2,3,3a,4,8b-hexahydrocyclopenta[*b*]indole by one excessive CH_2 group in indoline cycle (see, for example, dye **WS-2** and other similar dyes). Interestingly these higher PCE values for **MAX114** were achieved despite significant hypsochromic shift in the UV-vis spectrum and a slightly higher E_g than the **WS-2** dye. This can be explained by the changes of the E_{LUMO} and E_{HOMO} levels, which depend on the donor strength of the condensed alicyclic

fragment, affecting the degree of conjugation of the molecules and also on molecular geometry, changing in the transition from cyclopentene to cyclohexene derivative, which affects the delocalization of the charge. Surprisingly, replacement of the chalcogen atom in the central acceptor 2,1,3-benzochalcogenadiazole block from the sulfur atom to a more electronegative oxygen atom or a more voluminous selenium atom leads to nonlinear dependence with bathochromic shift (24-30 nm) in the UV-vis spectra, and bigger energy gap E_g of about 0.1 eV. Nevertheless, the exchange of oxygen- and selenium atoms in benzochalcogenadiazole to sulfur atom leads to a sharp increase in photovoltaic parameters, including PCE. In summary, the 9-(*p*-tolyl)-2,3,4,4a,9,9a-hexahydro-1*H*-carbazole donor building block opens new possibilities to improve the photovoltaic efficiency of organic sensitizers in DSSCs and demonstrates the importance of tuning also the non-conjugated aliphatic part of the donor group.

Acknowledgments

We gratefully acknowledge financial support from the Russian Science Foundation (grant no. 15-13-10022). We would also like to thank the Centre for Plastic Electronics (CPE) for support with the IPCE measurements. ET thanks JASSO for a PhD studentship.

Supplementary data

Supplementary data associated with this article can be found, in the online version, at …

References

[1] B. Oregan, M. Grätzel, A low-cost, high-efficiency solar cell based on dye sensitized colloidal TiO_2 films, Nature 353 (1991) 737-739.

[2] A. Hagfeldt, G. Boschloo, L. Sun, L. Kloo, H. Pettersson, Dye-Sensitized Solar Cells, Chem. Rev. 110 (2010) 6595-6663.

[3] A. Carella, F. Borbone, R. Centore, Research Progress on Photosensitizers for DSSC, Front. Chem. 6 (2018) article 481.

[4] C.-Y. Chen, M. Wang, J.-Y. Li, N. Pootrakulchote, L. Alibabaei, C. Ngoc-le, J.-D. Decoppet, J.-H. Tsai, C. Grätzel, C.-G. Wu, S. M. Zakeeruddin, M. Grätzel, Highly

efficient lightharvesting ruthenium sensitizer for thin-film dye-sensitized solar cells, ACS Nano 3 (2009) 3103-3109.

[5] S. Mathew, A. Yella, P. Gao, R. Humphry-Baker, B. F. E. Curchod, N. Ashari-Astani, I. Tavernelli, U. Rothlisberger, M. K. Nazeeruddin, M. Grätzel, Dye-sensitized solar cells with 13% efficiency achieved through the molecular engineering of porphyrin sensitizers, Nat. Chem. 6 (2014) 242–247.

[6] M. A. M. Al-Alwani, A. B. Mohamad, N. A. Ludin, A. H. Kadhum Abd, K. Sopian, Ren. Sust. Energy Rev. 65 (2016) 183-213.

[7] M. Liang, J. Chen, Arylamine organic dyes for dye-sensitized solar cells, Chem. Soc. Rev. 42 (2013) 3453-3488.

[8] R. Ilmi, A. Haque, M. S. Khan, High efficiency small molecule-based donor materials for organic solar cells, Org. Electron 58 (2018) 53-62.

[9] A. Mishra, M. K. R. Fischer, P. Bäuerle, Metal-free organic dyes for dye-sensitized solar cells: from structure: property relationships to design rules, Angew. Chem. Int. Ed. 48 (2009) 2474-2499.

[10] S. Chaurasia, J. T. Lin, Metal-free sensitizers for dye-sensitized solar cells, Chem. Rec. 16 (2016) 1311-1336.

[11] C.-P. Lee, C.-T. Li, K.-C. Ho, Use of organic materials in dye-sensitized solar cells, Mater. Today 20 (2017) 267-283.

[12] M. Liang, J. Chen, Arylamine organic dyes for dye-sensitized solar cells, Chem. Soc. Rev. 42 (2013) 3453-3488.

[13] T.-D. Kim, K.-S. Lee, Macromol. Rapid Commun. 36 (2015) 943-958.

[14] Y. Ooyama, Y. Harima, Photophysical and electrochemical properties, and molecular structures of organic dyes for dye-sensitized solar cells, ChemPhysChem 2012:13:4032-4080.

[15] P. Ganesan, A. Yella, T. W. Holcombe, P. Gao, R. Rajalingam, S. A. Al-Muhtase, M. Grätzel, M. K. Nazeeruddin, Unravel the impact of anchoring groups on the photovoltaic performances of diketopyrrolopyrrole sensitizers for dye-sensitized solar cells, ACS Sustainable Chem. Eng. 3 (2015) 2389-2396.

[16] W. H. Zhu, Y. Z. Wu, S. T. Wang, W. Q. Li, X. Li, J. Chen, Z. S. Wang, H. Tian, Organic D-A-π-A solar cell sensitizers with improved stability and spectral response, Adv. Funct. Mater. 21 (2011) 756-763.

[17] K. Pei, Y. Wu, W. Wu, Q. Zhang, B. Chen, H. Tian, W. Zhu, Constructing organic D-A-π-A-featured sensitizers with a quinoxaline unit for high-efficiency solar cells: the effect of an auxiliary acceptor on the absorption and the energy level alignment, Chem. Eur. J. 18 (2012) 8190–8200.

[18] W. Li, Y. Wu, Q. Zhang, H. Tian, W. Zhu, D-A-π-A featured sensitizers bearing phthalimide and benzotriazole as auxiliary acceptor: effect on absorption and charge recombination dynamics in dye-sensitized solar cells, ACS Appl. Mater. Interfaces 4 (2012) 1822-1830.

[19] L. Han, X. Zu, Y. Cui, H. Wu, Q. Ye, J. Gao, Novel D–A–π–A carbazole dyes containing benzothiadiazole chromophores for dye-sensitized solar cells, Org. Electron. 15 (2014) 1536-1544.

[20] Y. Z. Wu, W. H. Zhu. Organic sensitizers from D-π-A to D-A-π-A: effect of the internal electron-withdrawing units on molecular absorption, energy levels and photovoltaic performances, Chem. Soc. Rev. 42 (2013) 2039-2058.

[21] Y. Z. Wu, W. H. Zhu, S. M. Zakeeruddin, M. Grätzel, Insight into D-A-π-A structured sensitizers: a promising route to highly efficient and stable dye-sensitized solar cells, ACS Appl. Mater. Interfaces 7 (2015) 9307-9318.

[22] E. A. Knyazeva, O. A. Rakitin, Influence of structural factors photovoltaic properties of dye-sensitized solar cells, Russ. Chem. Rev. 85 (2016) 1146-1183.

[23] H.-X. Jia, Z.-S. Huang, L. Wanga, D. Cao, Quinoxaline-based organic dyes for efficient dye-sensitized solar cells: effect of different electron-withdrawing auxiliary acceptors on the solar cell performance, Dyes Pigm. 159 (2018) 8-17.

[24] E. A. Knyazeva, W. Wu, T. N. Chmovzh, N. Robertson, J. D. Woollins, O. A. Rakitin, Dye-sensitized solar cells: Investigation of D-A-π-A organic sensitizers based on [1,2,5]selenadiazolo[3,4-c]pyridine, Sol. Energy 144 (2017) 134-143.

[25] T. N. Chmovzh, E. A. Knyazeva, E. Tanaka, V. V. Popov, L. V. Mikhalchenko, N. Robertson, O. A. Rakitin, [1,2,5]Thiadiazolo[3,4-d]pyridazine as an internal acceptor in the D-A-π-A organic sensitizers for dye-sensitized solar cells, Molecules 24 (2019) article 1588.

[26] B. Xerri, F. Labat, K. Guo, S. Yang, C. Adamo, Investigating the role of the π-bridge characteristics in donor–π-spacer–acceptor type dyes for solar cell application: a theoretical study, Theor. Chem. Acc. 135 (2016) article 40.

[27] L. Zhang, J. M. Cole, Anchoring groups for dye-sensitized solar cells. ACS Appl. Mater. Interfaces 7 (2015) 3427-3455.

[28] Q. Chai, W. Li, J. Liu, Z. Geng, H. Tian, W.-h. Zhu, Rational molecular engineering of cyclopentadithiophene-bridged D-A-π-A sensitizers combining high photovoltaic efficiency with rapid dye adsorption, Scientific Rep. 5 (2015) article 11330.

[29] A. Baheti, P. Singh, C.-P. Lee, K. R. J. Thomas, K.-C. Ho 2,7-Diaminofluorene-based organic dyes for dye-sensitized solar cells: effect of auxiliary donor on optical and electrochemical properties. J. Org. Chem. 76 (2011) 4910-4920.

[30] Liang M, Chen J. Arylamine organic dyes for dye-sensitized solar cells. Chem Soc Rev 2013;42:3453-3488.

[31] R. Li, L. Xie, H. Feng, B. Liu, Molecular engineering of rhodanine dyes for highly efficient D-π-A organic sensitizer, Dyes Pigm. 156 (2018) 53-60.

[32] H. Song, J. Zhang, J. Jin, H. Wang, Y. Xie, Porphyrin sensitizers with modified indoline donors for dye-sensitized solar cells, J. Mater. Chem. C 6 (2018) 3927-3936.

[33] L. Han, J. Zhao, B. Wang, S. Jiang, Influence of π-bridge in N-fluorenyl indoline sensitizers on the photovoltaic performance of dye-sensitized solar cells, J. Photochem. Photobiol. A Chem. 326 (2016) 1-8.

[34] N. Shibayama, Y. Inoue, M. Abe, S. Kajiyama, H. Ozawa, H. Miura, H. Arakawa, Novel near-infrared carboxylated 1,3-indandione sensitizers for highly efficient flexible dye-sensitized solar cells, Chem. Commun. 51 (2015) 12795-12798.

[35] L. Wang, M. Liang, Y. Zhang, F. Cheng, X. Wang, Z. Sun, S. Xue, Influence of donor and bridge structure in D-A-π-A indoline dyes on the photovoltaic properties of dye-sensitized solar cells employing iodine/cobalt electrolyte, Dyes Pigm. 101 (2014) 270-279.

[36] B. Liu, B. Wang, R. Wang, L. Gao, S. Huo, Q. Liu, X. Li, W. Zhu, Influence of conjugated π-linker in D-D-π-A indoline dyes: towards long-term stable and efficient dye-sensitized solar cells with high photovoltage, J. Mater. Chem. A 2 (2014) 804-812.

[37] M. d. Akhtaruzzaman, A. Menggenbateer Islam, A. El-Shafei, N. Asao, T. Jin, L. Han, K. A. Alamry, S. A. Kosa, A. M. Asiri, Y. Yamamoto, Structure-property relationship of different electron donors: novel organic sensitizers based on fused dithienothiophene. π-conjugated linker for high efficiency dye-sensitized solar cells, Tetrahedron 69 (2013) 3444-3450.

[38] M. d. Akhtaruzzaman, Y. Seya, N. Asao, A. Islam, E. Kwon, A. El-Shafei, L. Han, Y. Yamamoto, Donor-acceptor dyes incorporating a stable dibenzosilole π-conjugated spacer for dye-sensitized solar cells, J. Mater. Chem. 22 (2012) 10771-10778.

[39] T. Dentani, Y. Kubota, K. Funabiki, J. Jin, T. Yoshida, H. Minoura, H. Miura, M. Matsui, Novel thiophene-conjugated indoline dyes for zinc oxide solar cells, New J. Chem. 33 (2009) 93-101.

[40] K. Saito, Y. Shibata, M. Yamanaka, T. Akiyama, Chiral phosphoric acid-catalyzed oxidative kinetic resolution of indolines based on transfer hydrogenation to imines. J. Amer. Chem. Soc. 135 (2013) 11740-11743.

[41] K. Pilgram, M. Zupan, R. Skiles, Bromination of 2,1,3-benzothiadiazoles, J. Heterocycl. Chem. 7 (1970) 629-633.

[42] N. Blouin, A. Michaud, D. Gendron, S. Wakim, E. Blair, R. Neagu-Plesu, M. Belletête, G. Durocher, Y. Tao, M. Leclerc, Toward a rational design of poly(2,7-carbazole) derivatives for solar cells, J. Amer. Chem. Soc. 130 (2008) 732-742.

[43] E. A. Knyazeva, T. N. Chmovzh, O. O. Ustimenko, G. R. Chkhetiani, I. S. Paleva, L. S. Konstantinova, L. V. Mikhal'chenko, O. A. Rakitin, Suzuki cross-coupling reactions of 4,7-dibromo[1,2,5]selenadiazolo[3,4-*c*]pyridine – a path to new solar cell components, Chem. Heterocyclic Comp. 53 (2017) 608-614.

[44] S. Fuse, S. Sugiyama, M. M. Maitani, Y. Wada, Y. Ogomi, S. Hayase, R. Katoh, T. Kaiho, T. Takahashi, Elucidating the structure-property relationships of donor-p-acceptor dyes for dye-sensitized solar cells (DSSCs) through rapid library synthesis by a one-pot procedure, Chem. Eur. J. 20 (2014) 10685-10694.

[45] C. M. Cardona, W. Li, A. E. Kaifer, D. Stockdale, G. C. Bazan, Electrochemical considerations for determining absolute frontier orbital energy levels of conjugated polymers for solar cell applications, Adv. Mater. 23 (2011) 2367-2371.

[46] P. Bujak, I. Kulszewicz-Bajer, M. Zagorska, V. Maurel, I. Wielgusa, A. Pron, Polymers for electronics and spintronics, Chem. Soc. Rev. 42 (2013) 8895-8999.

[47] G. Oskam, B. V. Bergeron, G. J. Meyer, P. C. Searson pseudohalogens for dye-sensitized TiO_2 photoelectrochemical cells, J. Phys. Chem. B 105 (2001) 6867-6873.

[48] D. P. Hagberg, T. Marinado, K. M. Karlsson, K. Nonomura, P. Qin, G. Boschloo, T. Brinck, A. Hagfeldt, L. Sun, Tuning the HOMO and LUMO energy levels of organic chromophores for dye sensitized solar cells, J. Org. Chem. 72 (2007) 9550-9556.

[49] B. Liu, W. Wu, X. Li, L. Li, S. Guo, X. Wei, W. Zhu, Q. Liu, Molecular engineering and theoretical investigation of organic sensitizers based on indoline dyes for quasi-solid state dye-sensitized solar cells, Phys. Chem. Chem. Phys. 13 (2011) 8985-8992.

[50] D. D. Babu, H. Cheema, D. Elsherbiny, A. El-Shafei, A. V. Adhikari, Molecular engineering and theoretical investigation of novel metal-free organic chromophores for dye-sensitized solar cells, Electrochim. Acta 176 (2015) 868-879.

[51] A. Hagfeldt, G. Boschloo, L. Kloo, H. Pettersson, Dye-sensitized solar cells. Chem. Rev. 110 (2010) 6595-6663.

[52] Y. Wu, X. Zhang, W. Li, Z.-S. Wang, H. Tian, W. Zhu, Hexylthiophene-featured D–A–π–A structural indoline chromophores for coadsorbent-free and panchromatic dye-sensitized solar cells. Adv. Energy Mater. 2 (2012) 149-156.